Catalysis Today 175 (2011) 40–47

Contents lists available at ScienceDirect

Catalysis Today

journal homepage: www.elsevier.com/locate/cattod

Dynamic oxygen mobility and a new insight into the role of Ni doping in $Pd/CeO_2–ZrO_2$ three-way catalysts

Guangfeng Li[a], Qiuyan Wang[a], Bo Zhao[a,b], Renxian Zhou[a,*]

[a] Institute of Catalysis, Zhejiang University, Hangzhou 310028, PR China
[b] School of Pharmaceutical and Chemical Engineering, Taizhou University, Taizhou 317000, PR China

ARTICLE INFO

Article history:
Received 8 October 2010
Received in revised form 18 April 2011
Accepted 23 April 2011
Available online 8 June 2011

Keywords:
Dynamic oxygen mobility
$Ce_{0.67}Zr_{0.33}O_2$
In situ Raman
Ni
Pd-only three-way catalyst

ABSTRACT

CZ doped by nickel oxide with different loadings was prepared through a co-precipitation and supercritical dried method and the corresponding Pd-only TWCs were prepared and characterized. The results demonstrate that Pd/CZNi(3%) catalyst exhibits the best catalytic activity and the widest operation window before and after aging, compared with that of other catalysts. Moreover, the introduction of nickel oxide with 3% loading increases the average pore diameter and broadens the range of pore size distribution of sample, which is propitious to the formation of accumulative pore favoring the adsorption/desorption of reaction species. The introduction of nickel oxide with suitable loading (3%) promotes the thermal stability of CZ corresponding to the better surface composition and more concentration of Ce^{3+} or oxygen vacancy. Furthermore, the introduction of nickel oxide with 3% loading exhibits the best DOSC compared with other content doping, possibly due to the better structure and better surface composition and better thermal stability of CZNi(3%).

1. Introduction

Regulations concerning automotive emissions are becoming more and more stringent in the most advanced countries, driving the industry to an effort to diminish the environmental impact of pollutants emitted by vehicles [1,2]. Three-way catalysts (TWCs) technology is considered as highly mature for automotive emission control and it is nearly 35 years on the market [2]. Commercial TWCs worked under oscillating feed gas composition around the stoichiometric value of air/fuel (A/F) ratio and continuously exposed to high temperatures tending to lose their catalytic activity and selectivity over time [3–5]. Cerium oxide (CeO_2) has been proven to improve the thermal stability of the support, increase the noble metal dispersion, and act as oxygen-storage capacity (OSC) under oscillating conditions and is extensively added to the currently used TWCs [6,7]. But it suffers from the drawback of thermal instability. $CeO_2–ZrO_2$ mixed oxide has potential applications as catalyst support due to its high surface area, thermal stability, and oxygen storage/release capacity [8]. $CeO_2–ZrO_2$ mixed oxide has been employed since 1994 in the cars and pioneered even earlier [2]. Pt and Rh are widely employed as active components in typical automotive TWCs. In general, Pt is associated with carbon monoxide and hydrocarbon oxidation, whereas nitrogen oxide reduction is mainly related to Rh [9,10]. Palladium as an active metal in TWCs has been known to have a good resistance to thermal sintering, a lower price than Rh and a higher activity for the oxidation of hydrocarbons and carbon monoxide [10,11]. In recent years, the introduction of transition metals into TWCs [12–15], which promoted the NO reduction and achieved the lower light-off temperature during the cold start phase, has earned much attention in Pd-only TWCs area [16–18]. Promising results have been obtained by using Mn, Cr or Cu, which have been attributed to the formation of the corresponding alloys. Terribile et al. [18] reported that both MnO_x and CuO at low loading dissolve within the ceria–zirconia lattice, which strongly influences the redox behavior of the catalysts by promoting low-temperature reduction of Ce^{4+}. A further promotional effect on catalytic property is observed with the introduction of MnO_x and CuO dissolved into $CeO_2–ZrO_2$ lattice. Moreover, homogeneity of the solid solution, structural features and composition are key factors in successful redox catalyst design. Furthermore, ternary solid solution could improve the thermal stability and enhance the migration and exchange of oxygen species by storing and/or releasing oxygen. In the present work, $Ce_{0.67}Zr_{0.33}O_2$ (CZ) doped by nickel oxide with different loadings was prepared through a co-precipitation and supercritical dried method and the corresponding Pd-only TWCs were prepared and characterized. In particular, we investigated the effect of nickel oxide doping on the pore structure of CZ, the redox behavior, dynamic oxygen storage/release capacity and catalytic performance of Pd-only TWCs using a combination of N_2 adsorption/desorption, X-ray photoelectron spectroscopy (XPS), in situ Raman, dynamic oxygen storage capacity (DOSC) and catalytic test.

* Corresponding author. Tel.: +86 571 88273290; fax: +86 571 88273283.
E-mail address: zhourenxian@zju.edu.cn (R. Zhou).

0920-5861/$ – see front matter.
doi:10.1016/j.cattod.2011.04.043

2. Experimental

2.1. Catalyst preparation

CZ doped by nickel oxide with different content was prepared through a co-precipitation and supercritical dried method. The doping of nickel oxide was fixed at x wt% (x = 0, 0.5, 1, 3, 5). $ZrO(NO_3)_2$, $Ce(NO_3)_3$ and $Ni(NO_3)_2{\cdot}6H_2O$ were used as metal precursors. The required amounts of $ZrO(NO_3)_2$, $Ce(NO_3)_3$ and/or $Ni(NO_3)_2{\cdot}6H_2O$ were dissolved in water. The NaOH solution was added dropwise to the solution of metal precursors to maintain the pH at about 9.5. The obtained slurry was aged at room temperature for 12 h, and then filtered, washed with deionized water and dried under supercritical condition in ethanol (265 °C, 7.0 MPa) for 2 h. The samples were calcined at 500 °C in air for 4 h to obtain fresh support. All of the obtained supports were pressed into pellets, crushed and sieved to 40–60 meshes. The supports were designated as CZ, CZNi(0.5%), CZNi(1%), CZNi(3%), CZNi(5%), respectively. All the samples were calcined at 1000 °C for 4 h in air to obtain aged supports.

Five Pd-only catalysts with different mixed oxides as supports (Pd/CZNi(x wt%), x = 0, 0.5, 1, 3 and 5) were prepared by incipient wetness impregnation method with aqueous solutions of H_2PdCl_4 as metal precursors. Pd content was 0.5 wt%. The impregnated sample was reduced with hydrazine hydrate solution for 2 h, washed several times with deionized water until no Cl^- ions detected in the filtered solution, and then dried at 110 °C for 4 h followed by calcination at 500 °C for 2 h to obtain fresh catalyst. The catalysts were further calcined at 1000 °C for 4 h in air to obtain aged catalyst.

2.2. Characterization techniques

The pore size distribution were determined by N_2 adsorption/desorption using TriStar Π 3020 (Micromeritics Inc.). The sample (0.15 g) was degassed at 200 °C for 3 h under vacuum, and N_2 adsorption was carried out at −196 °C.

XPS analysis was performed on a PHI5000c spectrometer with the Mg Kα radiation (1253.6 eV), operating at 14 kV and 20 mA. The surface charging effect was corrected by fixing the C 1s peak at a binding energy of 284.6 eV.

In situ Raman measurements of the samples were performed in a homemade in situ Raman cell linked to the Raman equipment. A Raman spectrum was recorded on a UV-HR Raman spectrograph with a He–Gd laser of 514 nm excitation wavelength. It consisted of two accumulations of 30 s with a resolution of 4 cm^{-1}. The sample was inserted in the cell and heated up to 500 °C under different atmosphere (O_2, NO_x and CO) with a heating rate of 10 °C min^{-1}. Prior to the measurement, each temperature was held for 10 min. Finally, the sample was cooled down to room temperature and a spectrum was collected again. For these two gases (NO_x and CO), after the spectra were collected at room temperature in the same atmosphere, the previous gas (NO_x and CO) was stopped and O_2 was introduced and the spectrum was collected again.

The dynamic oxygen storage capacity measurements with CO–O_2 pulses were obtained at 400 °C over about 25 mg sample. CO (4% CO/1% Ar/He at 300 mL/min for 10 s) and O_2 (2% O_2/1% Ar/He at 300 mL/min for 10 s) streams were pulsed alternately with a pulsation frequency (i.e., the number of CO and O_2 pulses per second) of 0.05 Hz until at least ten cycles.

2.3. Catalytic activity measurement

Catalytic tests were carried out with a fixed-bed continuous flow reactor. The catalyst (0.2 mL) was held in a quartz tube by packing quartz wool at both ends of the catalyst bed. The reaction mixture containing NO (0.1%), NO_2 (0.03%), C_3H_6 (0.067%), C_3H_8 (0.033%), CO (0.75%), O_2 (0.745%) and balance Ar was fed to the reactor at a GHSV of 43 000 h^{-1}. The effluent gas was analyzed by on-line Fourier transform infrared spectrophotometer (BRUKER EQ55) equipped with a multiple reflection transmission cell (Infrared Analysis Inc.; path length 10.0 m). All spectra were taken at a resolution of 2 cm^{-1} for 128 scans. The air/fuel ratio experiments were carried out at 400 °C. The concentration of O_2 was adjusted in the tests of air/fuel ratio from 850 ppm to 8440 ppm. The λ value of the simulated exhaust, which represents the ratio between the available oxygen and the oxygen needed for full conversion to CO_2, H_2O and N_2, is defined as $\lambda = \{2[O_2] + [NO] + 2[NO_2]\}/\{9[C_3H_6] + 10[C_3H_8] + [CO]\}$, $\lambda = 1$ was at stoichiometry and the corresponding concentration of O_2 was 7450 ppm.

3. Results and discussion

3.1. Catalytic performance of the catalysts

CZ doped by nickel oxide with different loadings was prepared through a co-precipitation and supercritical dried method and the corresponding Pd-only TWCs were examined by FTIR to analyze the effluent gas after three-way catalytic reaction. In our experiments, we also test the conversions of CO, HC and NO_x under different air/fuel ratios. W (λ value width) acts as another scale to evaluate catalyst property when CO, HC and NO_x conversions all reach to 80% under rich and lean conditions. Moreover, the wider the W value is, the broader the three-way working window is. Table 1 summarizes the light-off ($T_{50\%}$) and full-conversion temperatures ($T_{90\%}$) of HC, CO, NO and NO_2 as well as the width of the window (W) over fresh Pd/CZNi catalysts. From Table 1, it can be seen that the introduction of nickel oxide clearly promotes the catalytic activity and decreases the light-off temperature of the catalysts and broadens the three-way working window. Moreover, Pd/CZNi(3%) catalyst exhibits the best catalytic activity for CO elimination and the widest operation window compared with that of other catalysts. Furthermore,

Table 1
Light-off ($T_{50\%}$) and full-conversion ($T_{90\%}$) temperature of CO, HC, NO and NO_2 and the width of the window (W) over fresh Pd/CZNi(x wt%) catalysts.

Catalyst	$T_{50\%}$ (°C)				$T_{90\%}$ (°C)				W
	HC	CO	NO	NO_2	HC	CO	NO	NO_2	
Pd/CZ	258	178	246	195	283	204	284	233	0.221
Pd/CZNi(0.5%)	240	158	225	171	260	184	254	207	0.243
ΔT[a]	18	20	21	24	23	20	30	26	
Pd/CZNi(1%)	246	157	229	173	263	189	254	213	0.238
ΔT	12	21	17	22	20	15	30	20	
Pd/CZNi(3%)	263	140	240	180	285	170	279	221	0.250
ΔT	−5	38	6	15	−2	34	5	12	
Pd/CZNi(5%)	264	161	184	184	295	187	221	221	0.232
ΔT	−6	17	62	11	−12	17	63	12	

[a] $\Delta T = T(\text{Pd/CZ}) - T(\text{Pd/CZNi}(x\text{ wt\%}))$.

Table 2
Light-off ($T_{50\%}$) and full-conversion ($T_{90\%}$) temperature of CO, HC, NO and NO_2 and the width of the window (W) over aged Pd/CZNi(x wt%) catalysts.

Samples	$T_{50\%}$ (°C)				$T_{90\%}$ (°C)				W
	HC	CO	NO	NO_2	HC	CO	NO	NO_2	
Pd/CZ	288	180	272	202	303	219	302	240	0.2
Pd/CZNi(0.5%)	322	200	301	226	338	238	340	272	0.21
ΔT[a]	−34	−20	−29	−24	−35	−19	−38	−32	
Pd/CZNi(1%)	323	192	303	221	338	234	334	259	0.21
ΔT	−35	−12	−31	−19	−35	−15	−32	−19	
Pd/CZNi(3%)	284	166	257	186	298	201	295	229	0.26
ΔT	4	14	15	16	5	18	7	11	
Pd/CZNi(5%)	303	171	279	193	317	205	315	241	0.22
ΔT	−15	9	−7	9	−14	14	−13	−1	

[a] $\Delta T = T(\text{Pd/CZ}) - T(\text{Pd/CZNi}(x\,\text{wt\%}))$.

the introduction of nickel oxide with little loading (≤1%) strongly improves the catalytic activity of HC, CO, NO and NO_2. Table 2 summarizes the light-off ($T_{50\%}$) and full-conversion temperatures ($T_{90\%}$) of HC, CO, NO and NO_2 as well as the width of the window (W) over aged Pd/CZNi catalysts. From Table 2, we can conclude that only Pd/CZNi(3%) catalyst exhibits the promoting effect on the catalytic activity of samples after aging in accordance with the decrease of light-off and full-conversion temperatures, compared with that of aged Pd/CZ catalyst. Moreover, the operation window of activity of the catalyst becomes wider. The second good one is the aged Pd/CZNi(5%) catalyst. Aged Pd/CZNi(0.5%) and Pd/CZNi(1%) exhibit the worst catalytic activity. One possible explanation is that the introduction of nickel oxide with suitable loading (3%) promotes the thermal stability of CZ.

3.2. The characterization of samples

In order to understand the different catalytic performance with doping nickel oxide, we investigated the structure and the surface properties of CZ, CZNi(1%) and CZNi(3%) support and corresponding catalysts. The surface area of CZNi(1%) and CZNi(3%) is 147 and 152 m^2/g, respectively, which is larger than that of CZ (122 m^2/g). Moreover, the pore volume of CZNi(1%) and CZNi(3%) is 0.77 and 0.97 cm^3/g, respectively, which is larger than that of CZ (0.73 cm^3/g). The XRD patterns of the supports are depicted in Fig. 1. The cell parameter calculated from XRD of CZNi(0.5%), CZNi(1%), CZNi(3%), and CZNi(5%) is 0.5394, 0.5359, 0.5306 and 0.5382 nm, respectively, which is smaller than CZ (0.5407 nm). The crystallite size of CZNi(0.5%), CZNi(1%), CZNi(3%), and CZNi(5%) is 7.9, 7.9, 7.0, 6.2 and 7.3 nm, respectively. It may be due to the fact that the ion radius of Ni^{2+} (0.069 nm) is smaller than that of Ce^{4+} (0.097 nm)/Ce^{3+} (0.112 nm) and Zr^{4+} (0.084 nm). Incorporation of Ni^{2+} into the CZ lattice by replacing of Ce^{4+}/Ce^{3+} or Zr^{4+} leads to the shrinkage of the lattice parameter, especially for the CZNi(3%). It indicates the formation of Ce–Zr–Ni–O ternary solid solution between Ce, Zr and Ni. Additionally, the best symmetrical peaks and smallest crystal size are observed when the content of doped nickel oxide is 3%, confirming the formation of more homogeneous Ce–Zr–Ni–O ternary solid solution. The pore size distributions of fresh and aged supports are shown in Fig. 2. For fresh samples (Fig. 2A), the introduction of nickel oxide with 3% loading increases

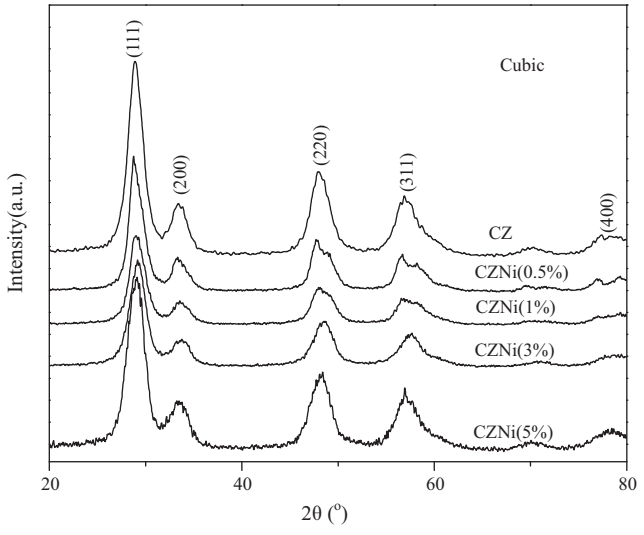

Fig. 1. XRD characterization of $Ce_{0.67}Zr_{0.33}O_2$ mixed oxides doped by nickel oxide with different content.

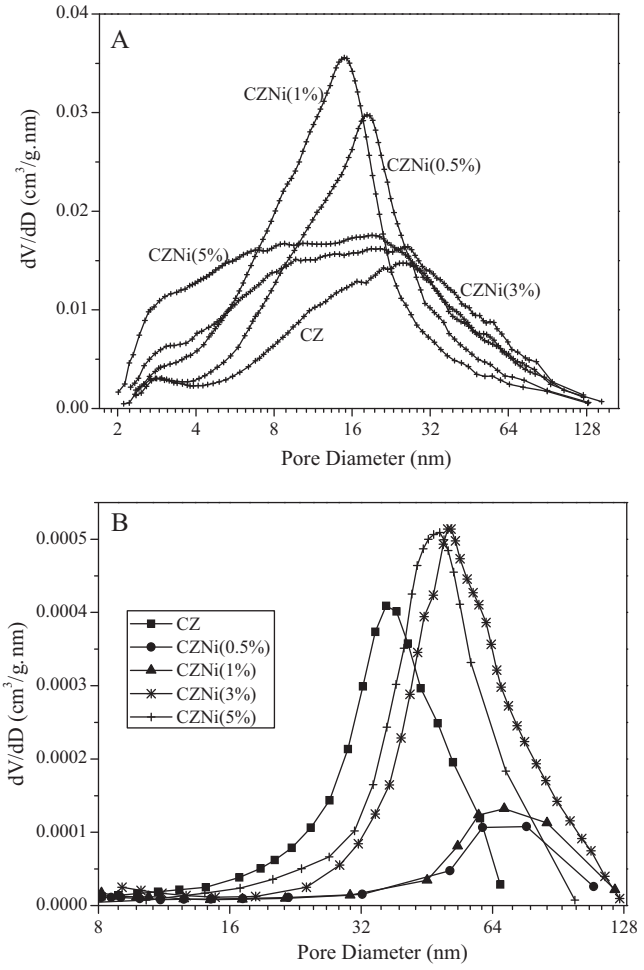

Fig. 2. Pore-size distribution of fresh (A) and aged (B) supports.

Table 3
Surface composition and surface atom ratios in the fresh and aged Pd/CZNi(*x* wt%) catalysts derived from XPS analysis.

Sample	Surface composition (at.%)					Ce/Zr	Ce^{3+} $3d_{5/2}$ in Ce(%)
	Ce 3d	Zr 3d	Ni 2p	Pd 3d	O 1s		
Fresh							
Pd/CZ	13.7	7.38	–	0.01	78.91	1.86	14.8
Pd/CZNi(1%)	16.2	7.29	0.3	0.01	76.2	2.22	15.5
Pd/CZNi(3%)	15.3	6.5	0.5	0.01	77.69	2.35	17.0
Aged							
Pd/CZ	8.58	8.34	–	0.01	83.07	1.03	12.2
Pd/CZNi(1%)	6.31	7.31	0.3	0.01	86.07	0.86	12.7
Pd/CZNi(3%)	6.71	5.82	0.4	0.02	87.07	1.15	13.7

the average pore diameter (23.3 nm) and broadens the range of pore size distribution, compared with that of CZ (20.8 nm). It may be due to the formation of accumulative pore, which favors the adsorption/desorption of reaction species. However, the range of pore size distribution becomes narrow when the doping content of nickel oxide is 1%. For aged samples as shown in Fig. 2B, we also can be seen that the introduction of nickel oxide with 3% loading increases the average pore diameter and broadens the range of pore size distribution. Moreover, the range of pore size distribution becomes narrow and the pore volume decreases over aged CZNi(1%) support, indicating that the severely sintering occurs after aging at 1000 °C. Combination with the discussion of fresh and aged supports and catalysts, we can speculate that the introduction of nickel oxide with suitable loading (3%) promotes the structure stability of CZ support corresponding to the better catalytic performance of catalyst.

The effects of nickel oxide doping on the oxidation state of Ce as well as on the surface atom ratios of Ce/Zr and Ce^{3+} $3d_{5/2}$ in Ce were investigated by means of the XPS technique and the results are presented in Table 3 and Fig. 3. As shown in Fig. 3, the curves of Ce 3d spectra over fresh and aged catalysts are composed of eight peaks corresponding to four pairs of spin–orbit doublets. The fitting and labeling of the peaks follows the convention [19–21]. Letters u and v refer to the $3d_{3/2}$ and $3d_{5/2}$ spin–orbit components, respectively. The couples corresponding to one of the two possible electron configuration of the final state of the Ce^{3+} species are labeled as u′ and v′. The relative percentage of the cerium species is obtained by the area ratio of Ce^{4+} $3d_{5/2}$ (v, v″ and v‴)/Ce^{3+} $3d_{5/2}$ (v′) [20,21]. The relative concentration of Ce^{3+} $3d_{5/2}$ in Ce is also obtained in Table 3. For fresh samples, the introduction of nickel oxide clearly promotes the ratio of Ce/Zr, especially for fresh Pd/CZNi(3%), indicating that part of surface Zr atoms is replaced by Ni atoms. Moreover, the relative concentration of Ce^{3+} $3d_{5/2}$ in Ce also increases with the introduction of nickel oxide, especially for fresh Pd/CZNi(3%) catalyst, indicating that the introduction of nickel oxide favors the transfer from Ce^{4+} to Ce^{3+} possibly due to the equilibrium of electric charge. We have known that the presence of Ce^{3+} is associated with the formation of oxygen vacancy [20,22]. Therefore, this observation to some extent indicates that the introduction of nickel oxide increases the oxygen vacancies of CZ support and further promotes the reduction of $Ce^{4+} \rightarrow Ce^{3+}$, especially for CZNi(3%). For aged samples, only Pd/CZNi(3%) exhibits higher ratio of Ce/Zr and increases more concentration of Ce^{3+} $3d_{5/2}$ in Ce, compared with that of Pd/CZ. It also indicates that the introduction of nickel oxide with suitable loading (3%) promotes the thermal stability of CZ corresponding to the better surface composition and more concentration of Ce^{3+} or oxygen vacancy.

3.3. *In situ Raman*

Figs. 4 and 5 show the in situ Raman spectra of the CZ and CZNi(3%) samples at different temperatures in O_2, NO_x and CO

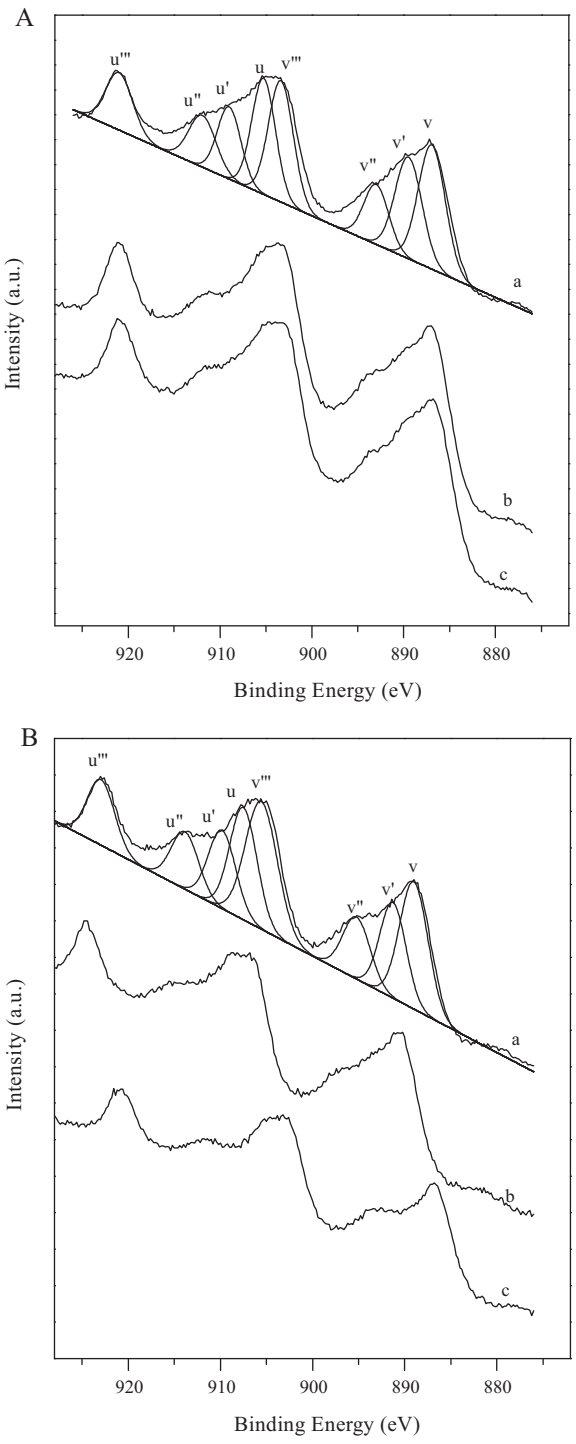

Fig. 3. Ce 3d spectra for the fresh (A) and aged (B) Pd/CZNi catalysts: (a) Pd/CZ, (b) Pd/CZNi(1%) and (c) Pd/CZNi(3%).

atmospheres with the 514 nm excitation laser line. In all spectra, two peaks are observed at 460 and 613 cm^{-1} which are attributed to the F_{2g} vibration mode of the fluorite structure of pure CeO_2 [23,24] and oxygen vacancies according to McBride et al. [25]. Moreover, the weak band at 246 cm^{-1} is also observed. The trend of the change of this band is consistent with that of the peak at 613 cm^{-1}, which could also be attributed to the asymmetric vibration caused by the formation of oxygen vacancies [26]. As reported in literature [23,24], the concentration of oxygen vacancies is determined by the ratio of the peak areas of the bands at 460 (A_{460}) and 613 cm^{-1}

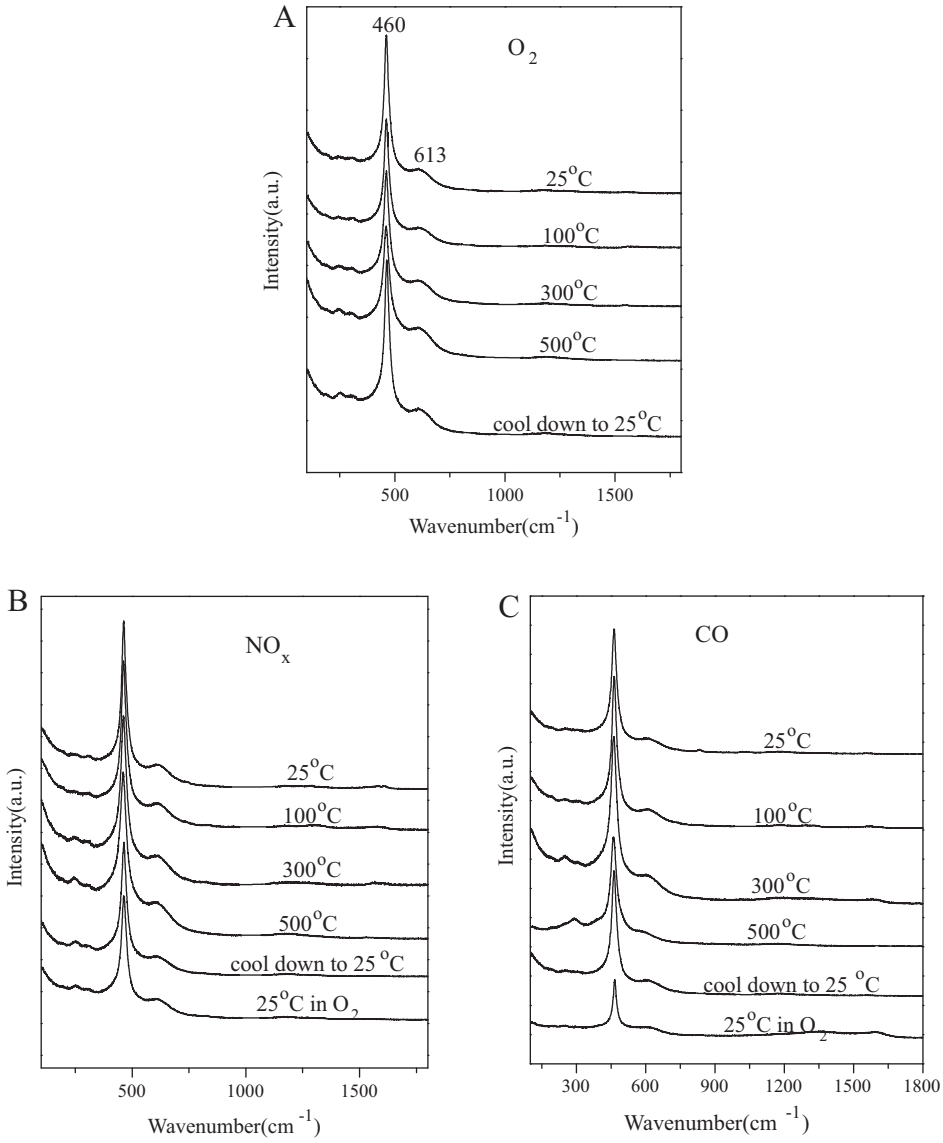

Fig. 4. In situ Raman spectra of fresh CZ under O_2 (A), NO_x (B) and CO (C) atmospheres with the 514 nm excitation laser line.

(A_{613}) based on the spectra in Figs. 4 and 5. The A_{613}/A_{460} value reflects the concentration of oxygen vacancies in the solid solution. The relationship between A_{613}/A_{460} and temperature under O_2, NO_x and CO atmospheres with the 514 nm excitation laser line is shown in Fig. 6. For CZ sample as shown in Fig. 6A, the value of A_{613}/A_{460} increases under O_2, while it first increases then decreases under NO_x and CO with increasing temperature. The A_{613}/A_{460} under NO_x is higher than that under O_2. It indicates that the mobility of oxygen under NO_x increases compared to that of under O_2. However, the value of A_{613}/A_{460} under CO is much lower compared to those under O_2 and NO_x, indicating that the atmosphere under CO makes against the transfer of oxygen over CZ support. It completely reverts when the sample is cooled down to room temperature in the previous atmosphere and exposed to O_2 (points 1 and 2). It indicates the oxygen storage and release properties of this sample. For CZNi(3%) sample shown in Fig. 6B, the values of A_{613}/A_{460} under all atmospheres are higher than that of CZ sample. It indicates that oxygen vacancy is formed when nickel oxide is doped into CZ lattice in order to maintain the electrical neutrality. The oxygen vacancies relating to structure modification is increased by the formation of more homogeneous structure, which has been proposed to explain the DOSC promotion. On the other hand, defects play another role in the oxygen storage process when noble metal is supported on ceria–zirconia, which is the usual application in practice. It also can be proved according to DOSC discussion below. It also can be seen that the value of A_{613}/A_{460} first increases then decreases under O_2, NO_x and CO with the increasing of temperature. Moreover, the value of A_{613}/A_{460} under CO is higher than that of under O_2 and NO_x below 500 °C over CZNi(3%), indicating that the introduction of Ni favors the transfer of oxygen in the atmosphere of CO. As CO is a strong reducing agent, the 613 cm^{-1} band merely changes under O_2 and NO_x, while it shows a clear shift toward higher frequency under CO, indicating a change in microstructure of the sample due to the reduction of Ce^{4+} or Fe^{3+} ions by CO, especially at high temperatures beyond 300 °C. Moreover, it also completely reverts when CZNi(3%) sample is cooled down to room temperature in the previous atmosphere and exposed to O_2 (points 1 and 2). It also indicates the oxygen storage and release properties of samples.

3.4. DOSC

One of the most important characteristics of TWCs is its ability to store oxygen under lean conditions (excess of oxygen) and release it under rich conditions (excess of fuel) [27,28]. Moreover,

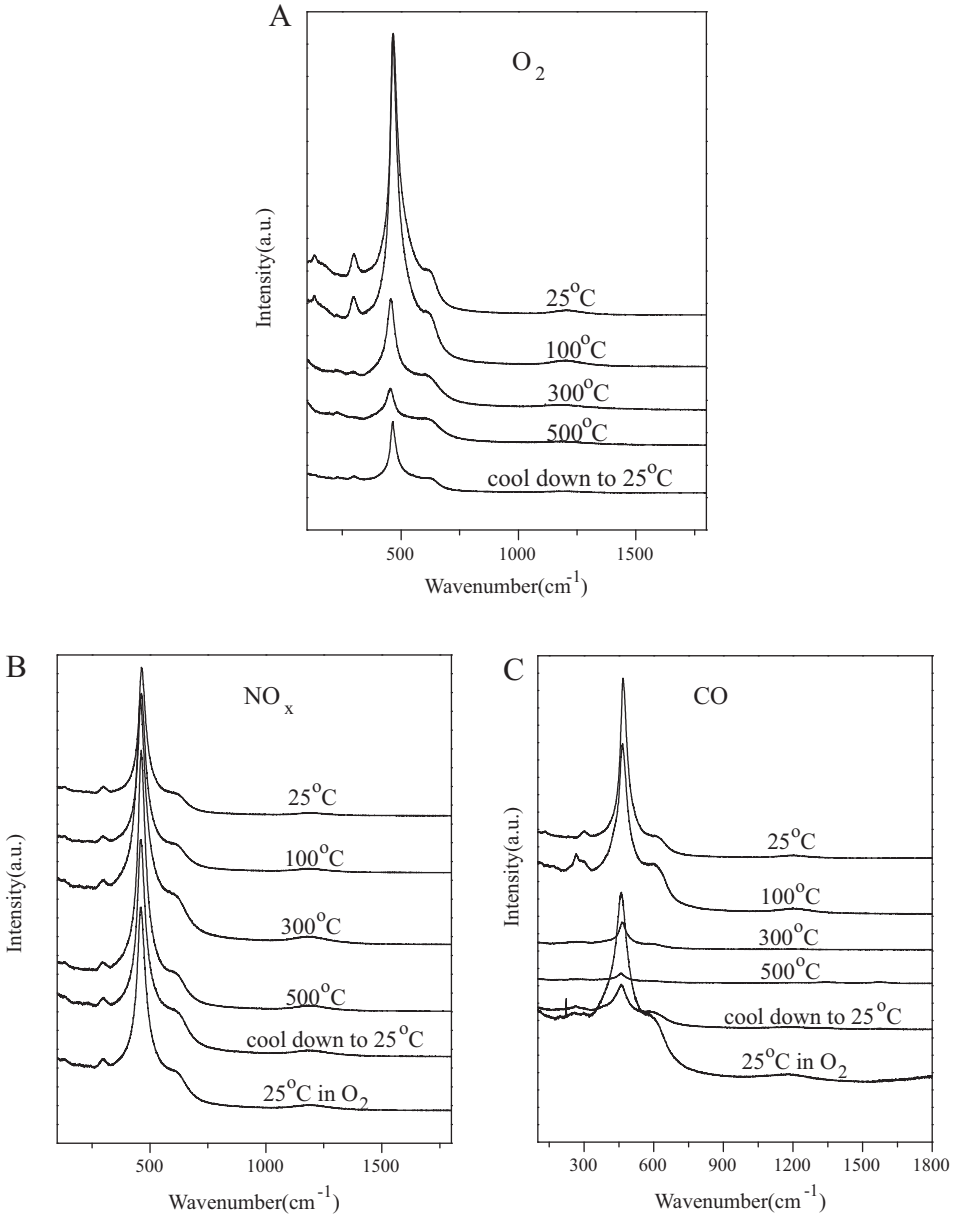

Fig. 5. In situ Raman spectra of fresh CZNi(3%) under O_2 (A), NO_x (B) and CO (C) atmospheres with the 514 nm excitation laser line.

this property, named oxygen storage capacity (OSC) is important for the accurate and effective functioning of TWCs and it was found to depend strongly on the available active metal sites being in close contact with ceria or $Ce_xZr_{1-x}O_2$ additives [3]. Thus, we investigated the DOSC of samples. Fig. 7 gives the representative transition curves with alternate dynamic pulses of 4%CO/1% Ar/He (10 s) and 2% O_2/1% Ar/He (10 s) over CZ and Pd/CZ samples. Two CO_2 peaks appear in a cycle. The first is originated from the reaction between CO and the storage oxygen of sample, and the second may be originated from the reaction between oxygen in gas phase and the adsorbed CO. The dynamic oxygen storage capacity of samples calculated from the dynamic pulse curves is shown in Fig. 8. For fresh supports, it can be seen that the introduction of nickel oxide clearly promotes the DOSC of CZ, especially for CZNi(3%), indicating that the interaction between Ce–Zr and Ni enhances the mobility of oxygen. We speculate that nickel oxide doping into CZ lattice by replacing the part of Zr atoms forms Ce–Zr–Ni–O ternary solid solution, which promotes the ability of store/release oxygen of support. It is known that the sensitivity of the DOSC characteristics to their surface composition and structure is an important aspect of the DOSC behavior of the ceria–zirconia-based materials. Moreover, the oxygen vacancies relating to structure modification is increased by the formation of more homogeneous structure, which has been proposed to explain the DOSC promotion. Based on the characterization of samples, we have obtained that the introduction of nickel oxide increases the oxygen vacancies of CZ support and further promotes the reduction of $Ce^{4+} \rightarrow Ce^{3+}$, especially for CZNi(3%), corresponding to the better surface composition and more concentration of Ce^{3+} or oxygen vacancy. Therefore, the introduction of nickel oxide with 3% loading exhibits the best DOSC compared with other content doping. Moreover, the excessive nickel oxide loading make against the formation of more homogeneous Ce–Zr–Ni–O structure and better surface composition, due to the conglomeration of nickel oxide. Thus, the dynamic oxygen storage capacity of samples decreases when the nickel oxide loading is 5%. Compared with fresh CZ and Pd/CZ, we can conclude that the loading of Pd clearly increases the DOSC of CZ support. It may be due to the fact that the oxidation of noble metal Pd in Pd/ceria–zirconia catalyst

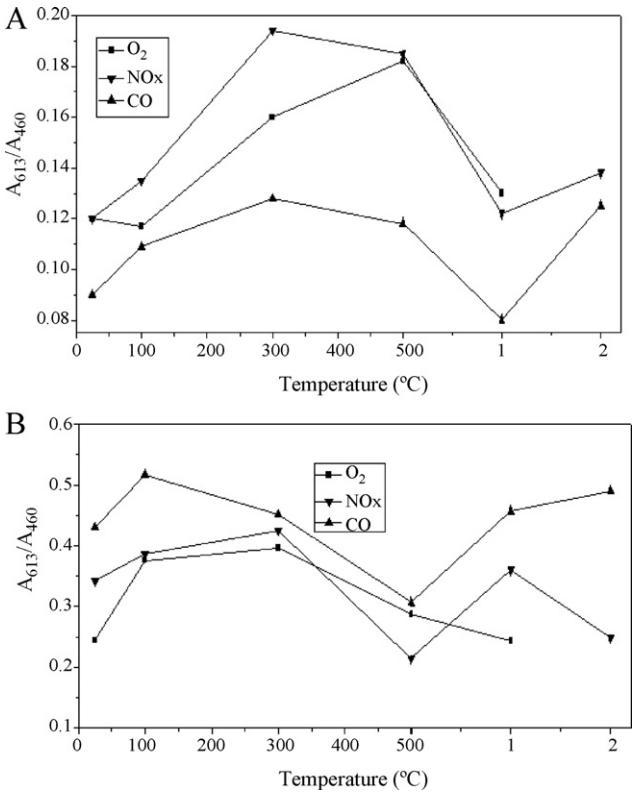

Fig. 6. Relationship between A_{613}/A_{460} and temperature with the 514 nm laser line under different atmospheres over CZ (A) and CZNi(3%) (B): (1) cool down to 25 °C in same atmosphere and (2) switch to O_2 after cooling down to 25 °C.

reflects the electron transfer from noble metal to ceria–zirconia, indicating that Ce is slightly reduced associating with the formation of oxygen vacancy [29,30]. Moreover, the introduction of nickel oxide promotes the electron transfer from noble metal Pd to Ce–Zr–Ni–O ternary solid solution in accordance with the enhancement of DOSC of catalyst compared with that of Pd/CZ, especially for Pd/CZNi(3%). After aging at 1000 °C, the introduction of nickel oxide also clearly increases the DOSC of CZ support, indicating that the formation of Ce–Zr–Ni–O ternary solid solution promotes the thermal stability of support, especially for aged CZNi(3%) support. Moreover, the DOSC of aged catalysts is surely higher than that of corresponding aged supports, indicating again that the oxidation of noble metal Pd in catalyst reflects the electron transfer from metal to support. Moreover, among all the samples examined, the introduction of nickel oxide with 3% loading exhibits the best DOSC compared with that of other content doping, which possibly due to the better structure and better surface composition and better thermal stability of CZNi(3%) support. Combined with the catalytic performance of fresh catalysts, we propose that the catalytic behavior of these bimetallic systems is strongly affected by the nature of support. The enhancement of the catalytic performance of Pd/CZNi may be due to the fact that the formation of more homogeneous Ce–Zr–Ni–O ternary solid solution in fresh CZNi promotes the surface composition and the DOSC of the sample, which further enhances the catalytic behavior of the catalyst. Moreover, the decrease of the surface composition and the DOSC of samples results in the deactivation of the aged catalysts. It indicates that the catalytic activity of catalyst could be correlated with the properties of the samples.

We also give the CO_2 response curves of fresh and aged samples as shown in Fig. 9. For fresh and aged supports, we can conclude that the start time of the CO_2 appearance over CZNi(3%) support is earlier than that of CZ, indicating that the CO_2 production rates for

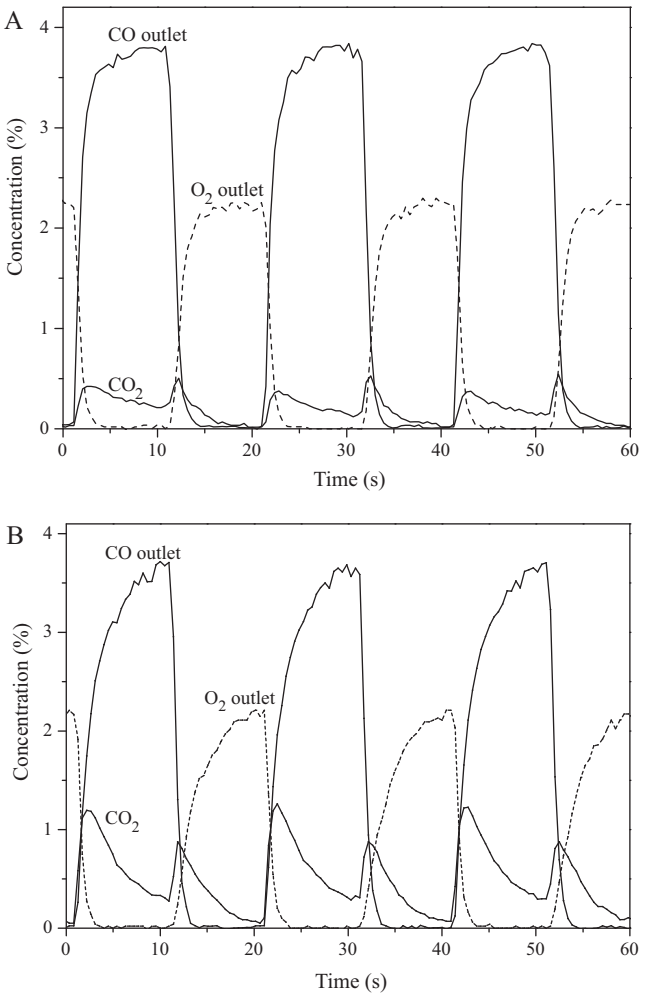

Fig. 7. Representative transition curve with alternate dynamic pulses of 4%CO/1% Ar/He (10 s) and 2% O_2/1% Ar/He (10 s) over CZ (A) and Pd/CZ (B).

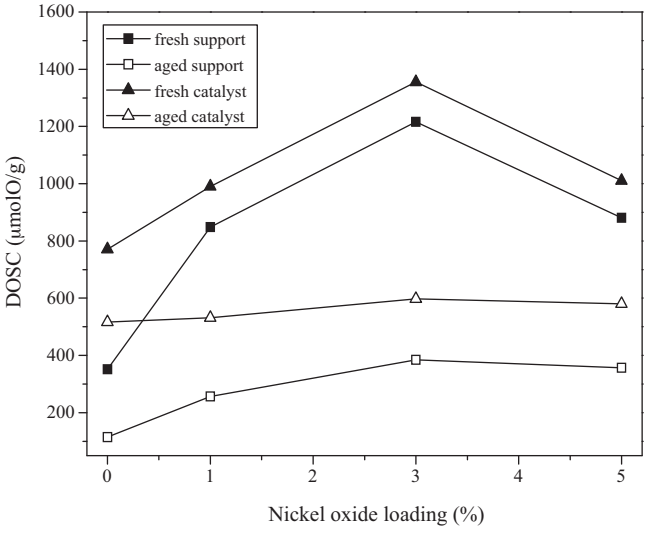

Fig. 8. Dynamic oxygen storage capacity of samples as a function of nickel oxide loading.

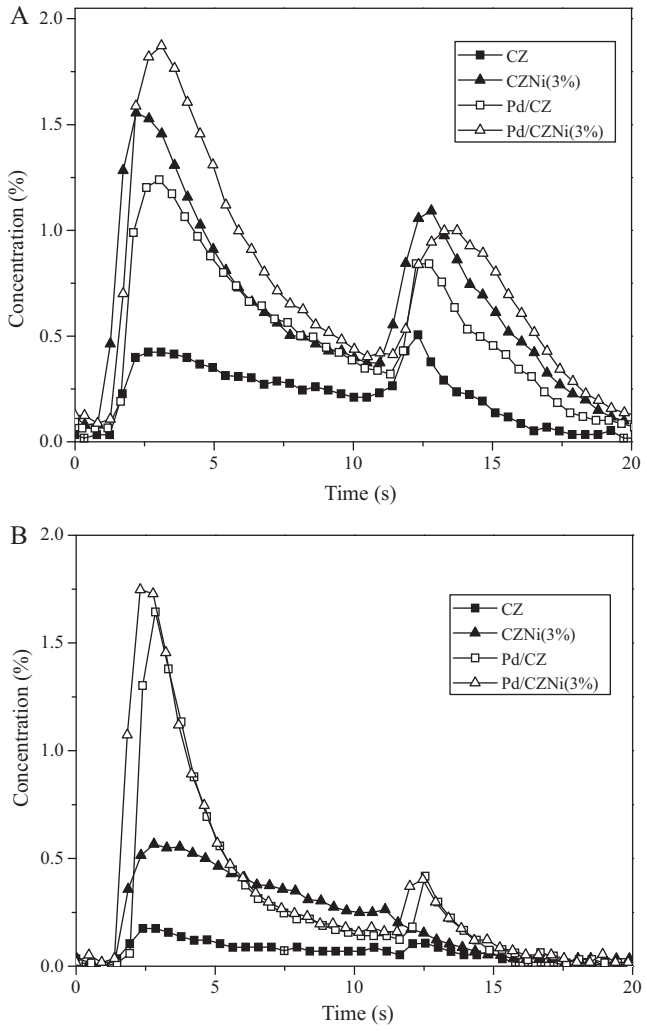

Fig. 9. CO_2 response curve of fresh (A) and aged (B) samples.

CZNi(3%) is more rapid compared with that of CZ. It may be due to the fact that the formation of Ce–Zr–Ni–O ternary solid solution is propitious to the promoting of surface reaction. Moreover, the start time of the CO_2 appearance over Pd/CZNi(3%) is earlier than that of Pd/CZ, indicating that the introduction of nickel oxide promotes the interaction between Ce–Zr and Pd. Furthermore, the interaction clearly promotes the oxygen mobility of samples.

4. Conclusion

CZ doped by nickel oxide with different loadings was prepared through a co-precipitation and supercritical dried method and the corresponding Pd-only TWCs were prepared and characterized using N_2 adsorption/desorption, XPS, in situ Raman, DOSC and catalytic test to analyze the effect of doping nickel oxide. The results demonstrate that Pd/CZNi(3%) catalyst exhibits the best catalytic activity in accordance with the decrease of light-off and full-conversion temperature and the widest operation window before and after aging, compared with that of other catalysts. It may be due to the fact that the introduction of nickel oxide with 3% loading increases the average pore diameter and broadens the range of pore size distribution, which is propitious to the formation of accumulative pore favoring the adsorption/desorption of reaction species. Moreover, the introduction of nickel oxide increases the oxygen vacancies of CZ support and further promotes the reduction of $Ce^{4+} \rightarrow Ce^{3+}$, especially for CZNi(3%). We have concluded that the introduction of nickel oxide with suitable loading (3%) promotes the thermal stability of CZ corresponding to the better surface composition and more concentration of Ce^{3+} or oxygen vacancy. The values of A_{613}/A_{460} under all atmospheres over CZNi(3%) are higher than that over CZ sample. It indicates that oxygen vacancy is formed when nickel oxide is doped into CZ lattice in order to maintain the electrical neutrality. It can also be proved by DOSC discussion. Moreover, the introduction of nickel oxide with 3% loading exhibits the best DOSC compared with other content doping, which possibly due to the better structure and better surface composition and better thermal stability of CZNi(3%) support.

Acknowledgements

We gratefully acknowledge the financial supports from the Ministry of Science and Technology of China (No: 2009AA064804). We gratefully acknowledge the Meiqing Shen professor's (from School of Chemical Engineering & Technology, Tianjin University) support of DOSC experiments.

References

[1] A. Iglesias-Juez, A. Martínez-Arias, M. Fernández-García, J. Catal. 221 (2004) 148–161.
[2] M. Shelef, R.W. McCabe, Catal. Today 62 (2000) 35–50.
[3] P.S. Lambrou, S.Y. Christou, A.P. Fotopoulos, F.K. Foti, T.N. Angelidis, A.M. Efstathiou, Appl. Catal. B: Environ. 59 (2005) 1–11.
[4] J.R. González-Velasco, J.A. Botas, R. Ferret, M.P. González-Marcos, J.L. Marc, M.A. Gutiérrez-Ortiz, Catal. Today 59 (2000) 395–402.
[5] P.S. Lambrou, C.N. Costa, S.Y. Christou, A.M. Efstathiou, Appl. Catal. B: Environ. 54 (2004) 237–250.
[6] R. Rajasree, J.H.B.J. Hoebink, J.C. Schouten, J. Catal. 223 (2004) 36–43.
[7] B. Azambre, L. Zenboury, F. Delacroix, J.V. Weber, Catal. Today 137 (2008) 278–282.
[8] J.-R. Kim, W.-J. Myeong, S.-K. Ihm, J. Catal. 263 (2009) 123–133.
[9] A. Suopanki, R. Polvinen, M. Valden, M. Härkönen, Catal. Today 100 (2005) 327–330.
[10] D.H. Kim, S. Ihl Woo, J.M. Lee, O.-B. Yang, Catal. Lett. 70 (2000) 35–41.
[11] J. Kašpar, P. Fornasiero, N. Hickey, Catal. Today 77 (2003) 419–449.
[12] J. Luo, M. Meng, J. Yao, X. Li, Y. Zha, X. Wang, T. Zhang, Appl. Catal. B 87 (2009) 92–103.
[13] L. Jia, M. Shen, J. Wang, X. Chu, J. Wang, Z. Hu, J. Rare Earths 26 (2008) 523–527.
[14] P.S. Lambrou, P.G. Savva, J.L.G. Fierro, A.M. Efstathiou, Appl. Catal. B 76 (2007) 375–385.
[15] P. Granger, C. Dujardin, J.-F. Paul, G. Leclercq, J. Mol. Catal. A 228 (2005) 241–253.
[16] A.B. Hungría, N.D. Browning, R.P. Erni, M. Fernández-García, J.C. Conesa, J.A. Pérez-Omil, A. Martínez-Arias, J. Catal. 235 (2005) 251–261.
[17] A. Martínez-Arias, M. Fernández-García, A.B. Hungría, A. Iglesias-Juez, J.A. Anderson, Catal. Today 126 (2007) 90–95.
[18] D. Terribile, A. Trovarelli, C. de Leitenburg, A. Primavera, G. Dolcetti, Catal. Today 47 (1999) 133–140.
[19] F.B. Noronha, E.C. Fendley, R.R. Soares, W.E. Alcarez, D.E. Resasco, Chem. Eng. J. 82 (2001) 21–31.
[20] J. Fan, X. Wu, X. Wu, Q. Liang, R. Ran, D. Weng, Appl. Catal. B 81 (2008) 38–48.
[21] J. Fan, D. Weng, X. Wu, X. Wu, R. Ran, J. Catal. 258 (2008) 177–186.
[22] C. Bozo, N. Guilhaume, J.-M. Herrmann, J. Catal. 203 (2001) 393–406.
[23] S.-P. Li, J.-Q. Lu, P. Fang, M.-F. Luo, J. Power Sources 193 (2009) 93–98.
[24] Z.-Y. Pu, J.-Q. Lu, M.-F. Luo, Y.-L. Xie, J. Phys. Chem. C 111 (2007) 18695–18702.
[25] J.R. McBride, K.C. Hass, B.D. Poindexter, W.H. Weber, J. Appl. Phys. 76 (1994) 2435–2441.
[26] M.F. Luo, Z.L. Yan, L.Y. Jin, J. Mol. Catal. A 260 (2006) 157–162.
[27] H.C. Yao, Y.F. Yu Yao, J. Catal. 86 (1984) 254–265.
[28] E.C. Su, C.N. Montreuil, W.G. Rothschild, Appl. Catal. 17 (1985) 75–86.
[29] M. Zhao, M. Shen, J. Wang, J. Catal. 248 (2007) 258–267.
[30] X. Wu, J. Fan, R. Rui, D. Weng, Chem. Eng. J. 109 (2005) 133–139.